On the Synthesis of Solar Coronal Emission Diagnostics

Steven R. Cranmer
Smithsonian Astrophysical Observatory, 60 Garden Street, Cambridge, MA 02138
February 20, 1997

1. Introduction

This set of notes has been compiled as an introduction to some of the basic theory behind the formation of spectral lines in the solar corona. The emphasis is mainly on ultraviolet spectral diagnostics which are observable with the Ultraviolet Coronagraph Spectrometer (UVCS) on the Solar and Heliospheric Observatory (SOHO) satellite. Although, for the most part, the derivations in these notes can be found elsewhere (see References), it is important to gather them together in a reasonably *ab initio* format at least once, if only for ease of later reference (and if only for the author!).

The remainder of these notes are organized as follows. In §2 we solve the equation of radiative transfer in the optically thin corona. Most of the physics of resonance line formation in the corona is contained within the scattering redistribution function, and this is derived in §3 for various physical situations. The standard approximations used to compute "Doppler dimming" of emission line strengths are then presented in §4. Finally, in Appendix A we set up the geometrical coordinate systems necessary to compute the emergent intensity from a 3D solar corona model, and in Appendix B we list the energies, opacities, and transition strengths of spectral lines of interest to UVCS observations.

2. Radiative Transfer in Spectral Lines

The interaction between radiation and matter is governed by the equation of radiative transfer, and here we examine this equation in the vicinity of a single spectral line transition. Following Mihalas (1978), Collins (1989), and others,

$$\frac{dI_\nu}{d\tau_\nu} = -I_\nu + S_\nu \quad , \tag{1}$$

where I_ν is the monochromatic specific intensity (in erg s^{-1} cm^{-2} sr^{-1} Hz^{-1}), S_ν is the source function of the radiation field, and τ_ν is the dimensionless optical depth, defined most generally along an arbitrary ray of path length x as

$$d\tau_\nu \; = \; \chi_{\rm tot} \, dx \quad . \tag{2}$$

The total opacity $\chi_{\rm tot}$ (in cm^{-1}), or inverse mean free path of photons, can be expressed as a sum of absorption and scattering interactions due to continuum and line processes:

$$\chi_{\rm tot} \; = \; \chi_C + \chi_L \phi(\nu) \; = \; [\sigma_C + \sigma_L \phi(\nu)] \; \rho(\mathbf{r}) \quad . \tag{3}$$

Subscripts C and L refer to continuum and line processes, and $\phi(\nu)$ is a profile function describing the frequency extent of the line (see §3). Because we assume the gas of electrons, atoms, and ions is tenuous enough to be treated as an ideal gas, individual microscopic interactions can be superposed linearly, and all contributions to $\chi_{\rm tot}$ depend on at least one power of the gas density ρ. Thus, the mass extinction coefficients σ (in cm^2 g^{-1}) are defined to be independent of the density of the medium.

The source function S_ν contains information about the local creation of photons along the ray, either by thermal emission or scattering into the ray. Mihalas (1978) gives, for a general two-level atom in the

presence of a background continuum in local thermodynamic equilibrium (LTE),

$$S_\nu \;=\; \frac{1}{\chi_{\rm tot}}\left[\chi_C B_\nu \;+\; \varepsilon\chi_L\phi(\nu)B_\nu + (1-\varepsilon)\chi_L\int_0^\infty d\nu' \oint \frac{d\Omega'}{4\pi}R(\nu',\hat{\mathbf{n}}';\nu,\hat{\mathbf{n}})I_{\nu'}(\Omega')\right] \quad , \tag{4}$$

where B_ν is the blackbody Planck function,

$$B_\nu(T) \;=\; \frac{2h\nu^3}{c^2}\left[\frac{1}{\exp(h\nu/kT)-1}\right] \tag{5}$$

and $R(\nu',\hat{\mathbf{n}}';\nu,\hat{\mathbf{n}})$ is the *redistribution function* which describes how individual line scatterings alter the frequencies and directions of the photons. The exact form of $R(\nu',\hat{\mathbf{n}}';\nu,\hat{\mathbf{n}})$, and how it is related to the line profile function $\phi(\nu)$, is described further in §3. The line thermalization parameter ε represents the fraction of line emission which occurs from thermal processes, and can be derived from the statistical equilibrium of the atom (see Appendix B).

The equation of radiative transfer has the formal solution

$$I_\nu(\tau_\nu) = \int_0^{\tau_\nu} S_\nu(t_\nu)e^{-(\tau_\nu - t_\nu)}dt_\nu \;+\; I_\nu^* e^{-\tau_\nu} \quad , \tag{6}$$

but for coronagraph observations of the solar wind, this solution can be simplified greatly. The incident "core" intensity I_ν^* is zero for rays not intercepting the solar photosphere, and the corona is often assumed to be optically thin ($\tau_\nu \ll 1$) for ultraviolet frequencies of interest. Thus,

$$I_\nu \;\approx\; \int_0^{\tau_\nu} S_\nu(t_\nu)\,[1-\tau_\nu+t_\nu]\,dt_\nu \tag{7}$$

$$\approx\; \int_0^{\tau_\nu} S_\nu\,dt_\nu \tag{8}$$

$$\approx\; \int_{x=-\infty}^{+\infty} \chi_{\rm tot}(x)\,S_\nu(x)\,dx \quad , \tag{9}$$

where x measures distance along the observed ray, with the observer at $x \to +\infty$. Because of the assumption that the corona is optically thin, the incident intensity $I_{\nu'}(\Omega')$ in eq. (4) can be approximated by an observed or empirical *solar disk* (usually chromospheric) intensity, thus uncoupling the radiative transfer. Equations (4) and (9) thus represent the fundamental quantities to evaluate for the emergent intensities and line profiles from coronal spectral lines.

3. Scattering Redistribution in a Spectral Line

The process of scattering, or atomic excitation followed by an immediate decay to the original state, is described completely for a given transition by the redistribution function $R(\nu',\hat{\mathbf{n}}';\nu,\hat{\mathbf{n}})$. In this Section we derive this function, first in the rest-frame of an atom, then taking account of the microscopic Doppler motions of an ensemble of atoms.

Define the frequencies of the absorbed and emitted photons, in the atom's frame, as ξ' and ξ, and their directions as $\hat{\mathbf{n}}'$ and $\hat{\mathbf{n}}$, respectively. The redistribution function $R(\xi',\hat{\mathbf{n}}';\xi,\hat{\mathbf{n}})$, which is normalized such that

$$\int_0^\infty d\xi' \int_0^\infty d\xi \oint \frac{d\Omega'}{4\pi}\oint \frac{d\Omega}{4\pi}R(\xi',\hat{\mathbf{n}}';\xi,\hat{\mathbf{n}}) \;=\; 1 \quad , \tag{10}$$

is a *probability density* of scattering from $(\xi',\hat{\mathbf{n}}')$ to $(\xi,\hat{\mathbf{n}})$. Assuming that the probabilities of angular and frequency redistribution are separable, we can write R as a product of two absorption probabilities (i.e.,

probabilities of obtaining the "initial state" $\xi', \hat{\mathbf{n}}'$) and two scattering probabilities (i.e., probabilities of actually redistributing from $\xi' \rightarrow \xi$ and $\hat{\mathbf{n}}' \rightarrow \hat{\mathbf{n}}$),

$$R(\xi', \hat{\mathbf{n}}'; \xi, \hat{\mathbf{n}}) \;=\; f(\xi')\, a(\hat{\mathbf{n}}') \;\cdot\; p(\xi', \xi)\, g(\hat{\mathbf{n}}', \hat{\mathbf{n}}) \;\; . \tag{11}$$

Following Hummer (1962) and Mihalas (1978), let us assume that on the atomic scale, there are no preferred directions, and that the absorption is *isotropic,* i.e., $a(\hat{\mathbf{n}}') = 1$. The angular redistribution $g(\hat{\mathbf{n}}', \hat{\mathbf{n}})$ can also be assumed to be isotropic, but the shapes of the atomic orbitals of the two levels can be used to specify it in more detail (Chandrasekhar 1960). For example, if one defines $\cos\Theta \equiv \hat{\mathbf{n}}' \cdot \hat{\mathbf{n}}$,

$$\begin{aligned} g(\hat{\mathbf{n}}', \hat{\mathbf{n}}) \;&=\; 1 \;\; , && \text{isotropic} \\ &=\; 3(1+\cos^2\Theta)/4 \;\; , && \text{dipole (e.g., Thomson or Rayleigh scattering)} \\ &=\; (11+3\cos^2\Theta)/12 \;\; , && \text{blended L}\alpha \text{ resonance doublet} \;\; , \end{aligned} \tag{12}$$

where the latter form was derived by House (1970), and has been utilized by Beckers & Chipman (1974) and Noci et al. (1987). These phase functions all follow the normalized form

$$g(\hat{\mathbf{n}}', \hat{\mathbf{n}}) \;=\; E + 3(1-E)\cos^2\Theta \;\; , \tag{13}$$

where for the above three cases, $E = 1$, $3/4$, and $11/12$, respectively.

The other two frequency-dependent functions in $R(\xi', \hat{\mathbf{n}}'; \xi, \hat{\mathbf{n}})$ are not as trivial to evaluate, and can be defined in various ways depending on the type of scattering particle.

3.1. Resonance Scattering

When photons interact with bound atoms and ions, the frequencies that are resonant with bound-bound transition energies undergo a significant amount of scattering. Hummer (1962) outlined four categories of redistribution that represent varying degrees of realism:

- **Case I:** An idealized atom with two perfectly sharp levels. Thus, $f(\xi') = \delta(\xi' - \nu_0)$, with ν_0 being the line-center frequency, and $p(\xi', \xi) = \delta(\xi' - \xi)$, implying perfect coherence in the atom's frame.

- **Case II:** An atom with a sharp lower state, but a naturally-broadened upper state reflecting its finite lifetime against radiative decay. The function $f(\xi')$ is thus given by a Lorentz profile

$$f(\xi') \;=\; L(\xi', \Gamma) \;\equiv\; \frac{1}{\pi}\frac{\Gamma/4\pi}{(\xi'-\nu_0)^2 + (\Gamma/4\pi)^2} \;\; , \tag{14}$$

  where Γ is the radiative damping rate of the upper level. (Note the factor of $1/\pi$, which is not commonly written explicitly, but is needed to retain the same normalization as a Dirac δ function in the limit $\Gamma \rightarrow 0$.) The transition in this case is still coherent, however, with $p(\xi', \xi)$ given as in Case I.

- **Case III:** Complete redistribution in the atom's frame. The lower and upper levels are as in Case II, but *collisions* with electrons are assumed so frequent that the electrons in the upper level are randomly reshuffled, and no correlation remains between ξ' and ξ. Thus, $f(\xi')$ is as in Case II, and $p(\xi', \xi) = L(\xi, \Gamma)$, independent of ξ'.

- **Case IV:** Subordinate redistribution between two broadened states. The excitation and de-excitation here must be treated as a single quantum mechanical process, so the previous assumption that $f(\xi')$ and $p(\xi', \xi)$ are two separate functions is not valid. See McKenna (1984) and Collins (1989) for various versions of the coupled function $f(\xi')p(\xi', \xi)$, which is too involved to reproduce here.

There is also Zanstra's (1946) intermediate approximation between Cases II and III, in which the lower level is sharp, but the upper level is broadened by both radiation damping and collisions. Defining $\gamma \equiv \Gamma_{\rm rad}/(\Gamma_{\rm rad}+\Gamma_{\rm coll})$, one can approximate this as

$$p(\xi',\xi) \;=\; \gamma\delta(\xi'-\xi) \;+\; (1-\gamma)\,L(\xi,\Gamma_{\rm rad}+\Gamma_{\rm coll}) \;\;. \tag{15}$$

Most applications to lines formed in the optically thin solar corona have assumed Case I redistribution, and the two Dirac delta functions for $f(\xi)$ and $p(\xi',\xi)$ are justified on the basis that the Doppler line widths in the $\sim 10^6$ K corona are much wider than most intrinsic natural or collisionally broadened profiles. A notable exception was the work of Cram & Vardavas (1978), who examined Case II redistribution in a simplified geometry, and found that it could subtly alter the interpretation of coronal line profiles. However, let us temporarily assume Case I for simplicity, and derive the redistribution function in an *observer's* frame.

Assuming the velocities of the atoms are nonrelativistic, the Doppler shifted laboratory-frame frequencies can be written

$$\nu' \;=\; \xi' + \frac{\nu_0}{c}\,\mathbf{v}\cdot\hat{\mathbf{n}}' \tag{16}$$

$$\nu \;=\; \xi + \frac{\nu_0}{c}\,\mathbf{v}\cdot\hat{\mathbf{n}} \tag{17}$$

and the general redistribution function *for a single atom* is

$$R_s(\nu',\hat{\mathbf{n}}';\nu,\hat{\mathbf{n}}) \;=\; f\left(\nu' - \frac{\nu_0}{c}\,\mathbf{v}\cdot\hat{\mathbf{n}}'\right)\; p\left(\nu' - \frac{\nu_0}{c}\,\mathbf{v}\cdot\hat{\mathbf{n}}'\;,\;\; \nu - \frac{\nu_0}{c}\,\mathbf{v}\cdot\hat{\mathbf{n}}\right)\; g(\hat{\mathbf{n}}',\hat{\mathbf{n}}) \;\;. \tag{18}$$

Finally, this function must be averaged over the microscopic velocity distribution of the atoms to obtain the actual observed redistribution,

$$R(\nu',\hat{\mathbf{n}}';\nu,\hat{\mathbf{n}}) \;=\; \int\!\!\int\!\!\int d^3\mathbf{v}\, F(\mathbf{v})\, R_s(\nu',\hat{\mathbf{n}}';\nu,\hat{\mathbf{n}}) \;\;, \tag{19}$$

and the velocity distribution is often given by a "drifting Maxwellian" (see, e.g., Dreicer 1959),

$$F(\mathbf{v}) \;=\; \left(\frac{\tilde{\beta}}{\pi}\right)^{3/2} \exp\left(-\tilde{\beta}|\mathbf{v}-\mathbf{u}|^2\right) \;\;, \tag{20}$$

where $\tilde{\beta} = m_A/2kT_A \equiv 1/v_{th}^2$, and $\mathbf{u}$ is the macroscopic bulk velocity of the gas. For Case I redistribution, the result of the above complicated integral is

$$R_I(\nu',\hat{\mathbf{n}}';\nu,\hat{\mathbf{n}}) \;=\; \frac{g(\hat{\mathbf{n}}',\hat{\mathbf{n}})}{\pi\beta(\Delta\nu_D)^2} \exp\left[-\zeta'^2\right]\, \exp\left[-\left(\frac{\zeta-\alpha\zeta'}{\beta}\right)^2\right] \tag{21}$$

(see Mihalas 1978 for details), where $\alpha = \cos\Theta$, $\beta = \sin\Theta$, $\Delta\nu_D = \nu_0 v_{th}/c$, and

$$\zeta \;\equiv\; \frac{\nu-\nu_0}{\Delta\nu_D} - \frac{\mathbf{u}\cdot\hat{\mathbf{n}}}{v_{th}} \tag{22}$$

$$\zeta' \;\equiv\; \frac{\nu'-\nu_0}{\Delta\nu_D} - \frac{\mathbf{u}\cdot\hat{\mathbf{n}}'}{v_{th}} \tag{23}$$

(see also Olsen et al. 1994 and Cranmer 1997 for other forms of the redistribution function). Note that $R_I(\nu',\hat{\mathbf{n}}';\nu,\hat{\mathbf{n}})$ is *symmetric* in ζ and ζ', which reflects the fact that the scattering is coherent in the atom's frame. Also, if $R_I(\nu',\hat{\mathbf{n}}';\nu,\hat{\mathbf{n}})$ is integrated over the absorbing frequency ν', one obtains

$$\int_0^\infty d\nu'\, R_I(\nu',\hat{\mathbf{n}}';\nu,\hat{\mathbf{n}}) \;=\; \frac{g(\hat{\mathbf{n}}',\hat{\mathbf{n}})}{\Delta\nu_D}\,\Phi(\zeta) \;\;, \tag{24}$$

where $\Phi(\zeta)$ is the dimensionless Doppler emission profile,

$$\Phi(\zeta) \equiv \frac{1}{\sqrt{\pi}} e^{-\zeta^2} \quad , \tag{25}$$

which is related to the line absorption profile $\phi(\nu)$ discussed in §2, via

$$\Phi(\zeta) = \Delta\nu_D \, \phi(\nu) \; ; \qquad \int_0^\infty d\nu \, \phi(\nu) = \int_{-\infty}^\infty d\zeta \, \Phi(\zeta) = 1 \; . \tag{26}$$

The lower limit of the integration over ζ is actually $-(\mathbf{u}\cdot\hat{\mathbf{n}} + c)/v_{th}$, but this is effectively $-\infty$ as far as the sharply-peaked emission profile is concerned.

3.2. Thomson Electron Scattering

The incident radiation from the solar photosphere and chromosphere scatters not only with atoms and ions, but with free electrons as well. In the nonrelativistic limit, when Compton frequency shifts are negligible, the photon redistribution can be characterized by coherency in the atom's frame, $p(\xi', \xi) = \delta(\xi' - \xi)$, and "gray" (i.e., frequency independent) absorption, $f(\xi') = 1$. With these definitions, the redistribution function is integrated over the velocity distribution (assumed Maxwellian, as above), and

$$R_e(\nu', \hat{\mathbf{n}}'; \nu, \hat{\mathbf{n}}) = \frac{g(\hat{\mathbf{n}}', \hat{\mathbf{n}})}{\sqrt{\pi}\,\Delta\nu_e} \frac{1}{\sqrt{2(1-\alpha)}} \exp\left[-\frac{(\zeta - \zeta')^2}{2(1-\alpha)}\right] \quad , \tag{27}$$

where $\Delta\nu_e = (\nu_0/c)\sqrt{2kT_e/m_e}$, the thermal width of the electron distribution. This result was originally derived by Dirac (1925), and also given by Mihalas (1978) and others. The opacity for this scattering process is given simply by

$$\chi_L = \sigma_T n_e = \left(\frac{8\pi e^4}{3m_e^2 c^4}\right) n_e = (6.6525 \times 10^{-25}\,\mathrm{cm}^2)\, n_e \quad . \tag{28}$$

In most coronal spectral lines, the electron-scattered component is negligibly weak when compared to the resonantly-scattered component. This can be seen by estimating the ratio of line-center emissivities (see Section 4),

$$\frac{j_\nu(\text{electron})}{j_\nu(\text{resonance})} \approx \frac{n_e}{n_i} \frac{\sigma_T}{(h\nu_0/4\pi)B_{ij}/\Delta\nu_D} \quad , \tag{29}$$

which is $\sim 10^{-4}$–10^{-3} for the Hydrogen Lα line. Note, however, that the electron-scattered profile is wider than the resonantly-scattered profile by a factor of $\sqrt{m_H/m_e} \approx 43$, so the ratio of *line-integrated* emissivities and intensities is larger by this amount.

4. Doppler Dimming Diagnostic Approximations

The formation of ultraviolet emission lines in the solar corona allows observers to deduce the velocity, density, and temperature of the various components of the outflowing solar wind plasma. Of particular note is the diagnostic of "Doppler dimming" (Hyder & Lites 1970; Beckers & Chipman 1974; Withbroe et al. 1982; Kohl & Withbroe 1982; Strachan et al. 1993), which allows wind velocities to be determined by the amount of Doppler shift between the incident chromospheric intensity and the moving coronal gas. The previous two Sections contain the radiative transfer equations required to compute this effect, but several further approximations allow them to be simplified to the point of obtaining analytic solutions. These solutions

should always be checked against the results of more exact numerical calculations, but they allow added insight into the physics of coronal line formation. Let us follow the notation of Noci et al. (1987), and develop the equations of Doppler dimming from the above radiative transfer.

Define the local *volume emissivity* j_ν (also denoted as η_ν) as the integrand of eq. (9), in the limit of an isolated pure-scattering spectral line ($\varepsilon = 0$) with an opacity much stronger than any neighboring continuum opacity ($\chi_L \gg \chi_C$):

$$j_\nu \equiv \chi_{\rm tot} S_\nu = \chi_L \int_0^\infty d\nu' \oint \frac{d\Omega'}{4\pi} R(\nu', \hat{\mathbf{n}}'; \nu, \hat{\mathbf{n}}) I_{\nu'}(\Omega') \ . \tag{30}$$

For Doppler dimming, we are primarily interested in the total line-integrated intensity, and in §4.1 we derive an approximate method of computing the decrease in this intensity due to the bulk motion of the solar wind. In §4.2, though, we examine the *frequency-dependent* emissivity, and find that the some of the key approximations used in §4.1 do not apply when actual line shapes need to be computed.

4.1. Line-Integrated Emission

Let us integrate the volume emissivity over the line frequency,

$$j \equiv \int_0^\infty j_\nu \, d\nu = \left(\frac{h\nu_0}{4\pi} n_i B_{ij} \right) \int_0^\infty d\nu \int_0^\infty d\nu' \oint \frac{d\Omega'}{4\pi} R(\nu', \hat{\mathbf{n}}'; \nu, \hat{\mathbf{n}}) I_{\nu'}(\Omega') \ , \tag{31}$$

where the line opacity χ_L has been replaced by the appropriate atomic constants and the lower-level number density n_i (see Appendix B).

Noci et al. (1987) proceed by making a critical assumption about the frequency dependence of the incident intensity $I_{\nu'}(\Omega')$, which amounts to a restatement of the Case I assumption of perfect coherence in the atom's frame, but replacing the microscopic velocity $\mathbf{v}$ with the macroscopic velocity $\mathbf{u}$. This is equivalent to assuming that $\zeta' = \zeta$, or

$$\nu' = \nu - \frac{\nu_0}{c} \mathbf{u} \cdot \hat{\mathbf{n}} + \frac{\nu_0}{c} \mathbf{u} \cdot \hat{\mathbf{n}}' \ . \tag{32}$$

With this substitution, the incident intensity can be brought outside the integration over ν' and eq. (24) can be used to evaluate this integral over the redistribution function alone, yielding

$$j = \frac{h\nu_0}{4\pi} n_i B_{ij} \int_0^\infty d\nu \oint \frac{d\Omega'}{4\pi} I \left(\nu - \frac{\nu_0}{c} \mathbf{u} \cdot \hat{\mathbf{n}} + \frac{\nu_0}{c} \mathbf{u} \cdot \hat{\mathbf{n}}' \right) g(\hat{\mathbf{n}}', \hat{\mathbf{n}}) \, \phi \left(\nu - \nu_0 - \frac{\nu_0}{c} \mathbf{u} \cdot \hat{\mathbf{n}} \right) \ . \tag{33}$$

For further simplicity let us assume that the scattering is perfectly isotropic, i.e., $g(\hat{\mathbf{n}}', \hat{\mathbf{n}}) = 1$, and that the radiation incident at the point in question comes solely from a "point source" at the center of the solar disk. Thus, $\hat{\mathbf{n}}' = \hat{\mathbf{e}}_r$ (see Appendix A), and the integral over solid angle reduces to

$$\oint \frac{d\Omega'}{4\pi} = \frac{1 - \sqrt{1 - (R_\odot^2 / r^2)}}{2} \approx \frac{R_\odot^2}{4r^2} \ , \tag{34}$$

and

$$j \approx \frac{h\nu_0}{4\pi} n_i B_{ij} \frac{R_\odot^2}{4r^2} \int_0^\infty d\nu \ I \left(\nu - \frac{\nu_0}{c} \mathbf{u} \cdot \hat{\mathbf{n}} + \frac{\nu_0}{c} \mathbf{u} \cdot \hat{\mathbf{n}}' \right) \phi \left(\nu - \nu_0 - \frac{\nu_0}{c} \mathbf{u} \cdot \hat{\mathbf{n}} \right) \ . \tag{35}$$

Finally, define a translated frequency variable

$$\tilde{\nu} \equiv \nu - \frac{\nu_0}{c} \mathbf{u} \cdot \hat{\mathbf{n}} \ , \qquad d\tilde{\nu} = d\nu \ , \tag{36}$$

substitute it into eq. (35), and rename $\tilde{\nu} \rightarrow \nu$. Thus,

$$j \approx \frac{h\nu_0}{4\pi} n_i B_{ij} \frac{R_\odot^2}{4r^2} \int_0^\infty d\nu \; I\left(\nu + \frac{\nu_0}{c}\mathbf{u}\cdot\hat{\mathbf{n}}'\right) \phi\left(\nu - \nu_0\right) \quad , \tag{37}$$

which is proportional to the simplified factor $F(\delta\lambda)$ presented in the Appendix of Noci et al. (1987).

Defining the "Doppler dimming factor" $D(\mathbf{u}) \equiv j(\mathbf{u})/j(0)$, we obtain the asymptotic expression

$$D(\mathbf{u}) \approx \frac{\int_0^\infty d\nu \, I(\nu + \delta\nu) \, \phi(\nu - \nu_0)}{\int_0^\infty d\nu \, I(\nu) \, \phi(\nu - \nu_0)} \quad , \tag{38}$$

where $\delta\nu = \nu_0 \mathbf{u}\cdot\hat{\mathbf{n}}'/c$. In many situations, both the incident intensity I and the profile function ϕ can be assumed Gaussian, i.e.,

$$I(\nu) = I_0 \exp\left[-\left(\frac{\nu-\nu_0}{\Delta\nu_I}\right)^2\right] \quad , \qquad \phi(\nu-\nu_0) = \frac{1}{\Delta\nu_D\sqrt{\pi}} \exp\left[-\left(\frac{\nu-\nu_0}{\Delta\nu_D}\right)^2\right] \quad , \tag{39}$$

and, in this case, $D(\mathbf{u})$ is evaluated analytically:

$$D(\mathbf{u}) = \exp\left[\frac{-(\delta\nu)^2}{(\Delta\nu_I)^2 + (\Delta\nu_D)^2}\right] \tag{40}$$

or in terms of wavelengths,

$$D(\mathbf{u}) = \exp\left[\frac{-(\delta\lambda)^2}{(\Delta\lambda_I)^2 + (\Delta\lambda_D)^2}\right] \quad , \tag{41}$$

with $\delta\lambda = -\lambda_0 \mathbf{u}\cdot\hat{\mathbf{n}}'/c$, and $\Delta\lambda = -(\lambda_0^2/c)\Delta\nu$. In the case of "Doppler enhanced pumping" by intensity from a neighboring line (Noci et al. 1987), the incident intensity can be represented by a sum of two components,

$$I(\nu) = I_0 \exp\left[-\left(\frac{\nu-\nu_0}{\Delta\nu_I}\right)^2\right] + I_P \exp\left[-\left(\frac{\nu-\nu_0+\Delta\nu_N}{\Delta\nu_P}\right)^2\right] \quad , \tag{42}$$

and

$$D(\mathbf{u}) = \frac{\exp[-(\delta\nu)^2/(\Delta\nu_I^2 + \Delta\nu_D^2)] + P\exp[-(\delta\nu+\Delta\nu_N)^2/(\Delta\nu_P^2+\Delta\nu_D^2)]}{1 + P\exp[-(\Delta\nu_N)^2/(\Delta\nu_P^2+\Delta\nu_D^2)]} \tag{43}$$

where

$$P = \frac{I_P \, \Delta\nu_P}{I_0 \, \Delta\nu_I} \sqrt{\frac{(\Delta\nu_I)^2 + (\Delta\nu_D)^2}{(\Delta\nu_P)^2 + (\Delta\nu_D)^2}} \quad . \tag{44}$$

Figure 1 displays the analytic Doppler dimming functions $D(\mathbf{u})$ for three lines of interest to UVCS, using the incident intensity data from Table 2, in Appendix B. Note that we assume the wind velocity is purely radial and always parallel to the incident radiation vector $\hat{\mathbf{n}}'$, and thus $\mathbf{u}\cdot\hat{\mathbf{n}}' = u_r$. Note also the similarity to, e.g., Figure 2 of Kohl et al. (1995), which contains Doppler dimming functions computed with more sophisticated methods.

4.2. Emission Line Profiles

Let us examine the consequences on the *line-shape* of the critical approximation (eq. [32]) made by Noci et al. (1987). Under this approximation, the monochromatic emissivity is given by the integrand of eq. (37), which can be written schematically as

$$j_\nu \propto I(\nu + \delta\nu) \, \phi(\nu - \nu_0) \quad . \tag{45}$$

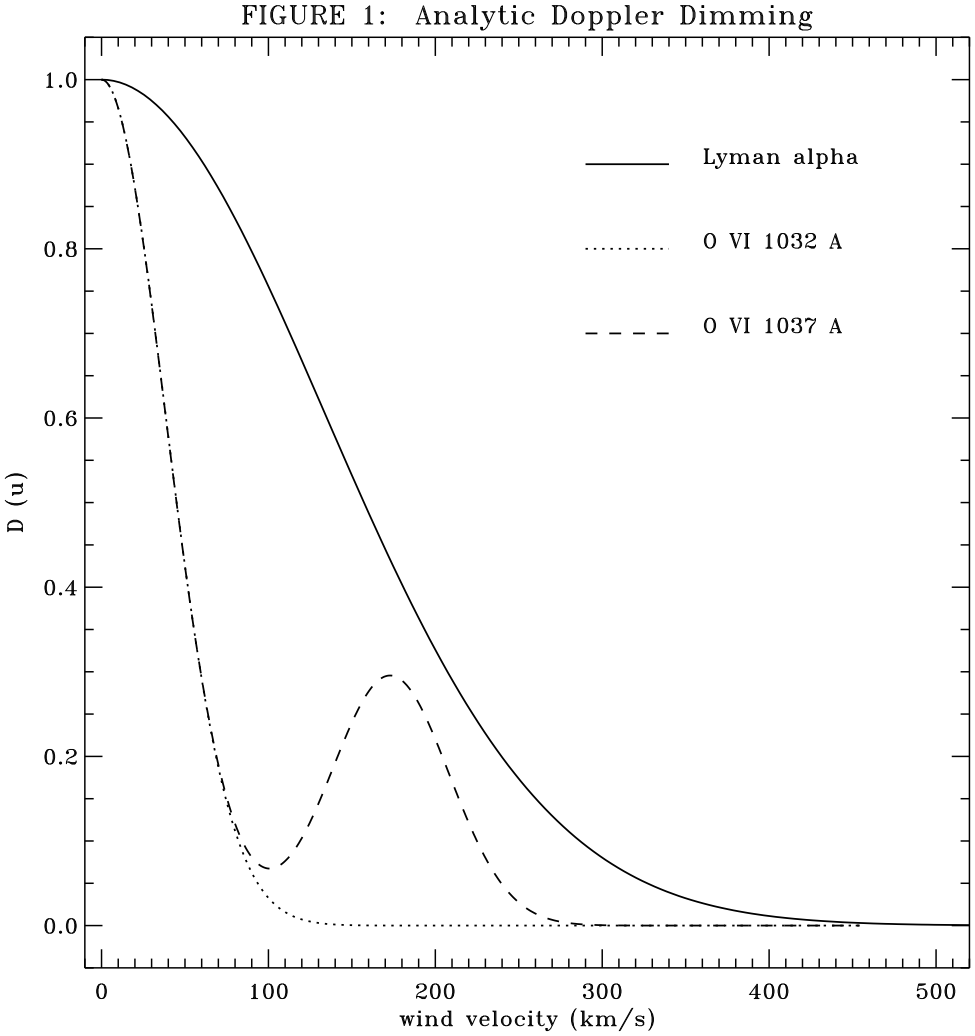

Fig. 1.— Analytic Doppler dimming functions for Lyman alpha (solid line), O VI 1032 Å (dotted line), and O VI 1037 Å (dashed line). The latter is "pumped" by the incident intensity from a neighboring C II line.

Let us further assume that the incident intensity I and the profile function ϕ can be assumed Gaussian, as above in eq. (39), and also that $\Delta\nu_D = \Delta\nu_I \equiv \Delta\nu$, for simplicity. Thus, j_ν can be shown to depend on

$$j_\nu \propto \exp\left[-2\left(\frac{\nu-\nu_0}{\Delta\nu}+\frac{\delta\nu}{2\Delta\nu}\right)^2-\frac{1}{2}\left(\frac{\delta\nu}{\Delta\nu}\right)^2\right] \quad , \tag{46}$$

which is centered about a frequency $\nu = \nu_0 - \delta\nu/2$, *not* the line-center frequency ν_0.

Is this result realistic? Observations of coronal ultraviolet emission lines do not show appreciable line-shifts due to the bulk velocity of the solar wind. Let us re-derive the frequency-dependence of the above emissivity *without* the Noci et al. (1987) approximation. However, in order to arrive at an analytic result, we will examine the scattering at one preferred point along the line of sight: $x = 0$, $r = b$, i.e., 90° scattering (see Appendix A). This is crudely justified by noting that, for optically thin lines, the maximal contribution along the line of sight occurs for points with the highest density, and thus closest to the star. At the 90°-scattering point, $\alpha = 0$, $\beta = 1$, $\mathbf{u}\cdot\hat{\mathbf{n}} = 0$, and $\mathbf{u}\cdot\hat{\mathbf{n}}' = u_r$. Thus, the scaled frequency variables are given simply by

$$\zeta = \frac{\nu-\nu_0}{\Delta\nu_D} \quad , \qquad \zeta' = \frac{\nu'-\nu_0}{\Delta\nu_D}-\frac{u_r}{v_{th}} \quad . \tag{47}$$

For isotropic scattering ($g(\hat{\mathbf{n}}',\hat{\mathbf{n}}) = 1$), the Case I redistribution function is

$$R_I = \frac{1}{\pi(\Delta\nu_D)^2}\exp(-\zeta'^2)\exp(-\zeta^2) \quad , \tag{48}$$

which is equivalent to complete redistribution (CRD) in the observer's frame.

The volume emissivity j_ν is given by integrating the product of the redistribution function and the incident intensity over the primed frequency variable ν', and for a Gaussian incident intensity profile (eq. [39]), this yields

$$j_\nu = \frac{I_0\chi_L}{\sqrt{\pi}}\left(\frac{R_\odot^2}{4r^2}\right)\frac{(\Delta\nu_I/\Delta\nu_D)}{\sqrt{\Delta\nu_I^2+\Delta\nu_D^2}}\exp\left[-\left(\frac{\nu-\nu_0}{\Delta\nu_D}\right)^2-\frac{(\delta\nu)^2}{\Delta\nu_I^2+\Delta\nu_D^2}\right] \tag{49}$$

$$\propto \phi(\nu-\nu_0)\,D(\mathbf{u}) \quad . \tag{50}$$

This emissivity is centered about ν_0, and not anomalously shifted as under the above approximation.

The above indicates that the dominant contribution to a resonantly-scattered optically-thin emission line, from ∼90° scattering, is from the local absorption profile (in this case a Gaussian with Doppler width $\Delta\nu_D$), and is Doppler-dimmed in a similar way as the results of the line-integrated analysis of §4.1. However, let us examine the cases of 45° and 135° scattering to evaluate the importance of other rays along the line of sight. For these two symmetric points, $x = \pm b$, $r = b\sqrt{2}$, and we denote the forward (backward) scattering points by the upper (lower) sign.

Thus, $\alpha = \pm 1/\sqrt{2}$, $\beta = 1/\sqrt{2}$, and the scaled frequency variables are given by

$$\zeta = \frac{\nu-\nu_0}{\Delta\nu_D}\mp\frac{u_r}{v_{th}\sqrt{2}} \quad , \qquad \zeta' = \frac{\nu'-\nu_0}{\Delta\nu_D}-\frac{u_r}{v_{th}} \quad . \tag{51}$$

After some manipulation, the Case I redistribution function is

$$R_I = \frac{\sqrt{2}}{\pi(\Delta\nu_D)^2}\exp[-2\zeta^2 \pm 2\sqrt{2}\zeta\zeta' - 2\zeta'^2] \quad , \tag{52}$$

and the integration over the primed frequency variable ν' yields the volume emissivity. Neglecting frequency-independent constants, and assuming again for simplicity that $\Delta\nu_D = \Delta\nu_I \equiv \Delta\nu$, one obtains

$$j_\nu \propto \exp\left[-\frac{4}{3}\left(\frac{\nu-\nu_0}{\Delta\nu}\mp\frac{\delta\nu}{\Delta\nu\sqrt{2}}\right)^2\right] \quad . \tag{53}$$

Thus, the emergent line profiles from these two "offset" points along the line of sight are symmetrically blue/red-shifted from line-center by $\pm\delta\nu/\sqrt{2}$. These profiles are also *narrower* by a factor of $\sqrt{3}/2$ than the profile at line-center, which can be understood by the presence of the β in the denominator of the one of the exponents in R_I. In the limit of pure forward or backward scattering (i.e., by 0° and 180°) which occurs infinitely far from the star, $\beta \rightarrow 0$, implying that the lines grow infinitesimally thin.

The end result of this analysis is that the line profiles formed by integrating j_ν over the line of sight should be symmetric about line-center, but deviate slightly from a Gaussian shape because of the blue/red-shifted components at scattering angles differing significantly from 90°. Numerical integrations for Case I redistribution produce line profiles slightly narrower than Gaussians, which can be fit by "quasi-Gaussian" functions of the form

$$Q(\nu) \;=\; Q_0 \exp\left(-\left|\frac{\nu-\nu_0}{\Delta\nu}\right|^n\right) \quad , \tag{54}$$

where nonlinear least-squares fitting gives $n \approx 1.8$–1.9.

Cram & Vardavas (1978), who examined Case II redistribution in optically-thin emission lines, found that emergent line profiles become slightly *asymmetric* about line-center due to the Lorentzian atomic absorption profile. This effect can be understood in a straightforward way by assuming 90° scattering, as above. However, if the incident intensity $I(\nu')$ is taken to have a Gaussian profile, the integration over ν' cannot be computed analytically. Let us therefore assume the incident intensity profile is proportional to a Dirac delta function, $\delta(\nu'-\nu_0)$. (Note that this assumption recovers many of the same results for Case I redistribution as above.) Thus, in this case,

$$\begin{aligned} j_\nu \;&\propto\; R_{II}(\nu_0,\hat{\mathbf{e}}_r;\nu,\hat{\mathbf{n}}) \\ &\propto\; \exp\left[-\frac{1}{2}\left(\frac{\nu-\nu_0}{\Delta\nu_D}+\frac{\delta\nu}{\Delta\nu_D}\right)^2\right]\; H\left[a\sqrt{2}\,,\;\frac{1}{\sqrt{2}}\left(\frac{\nu-\nu_0}{\Delta\nu_D}-\frac{\delta\nu}{\Delta\nu_D}\right)\right] \quad . \end{aligned} \tag{55}$$

The asymmetry in this emission profile becomes evident if one examines, e.g., the two red/blue-shifted frequencies $\nu = \nu_0 \pm \delta\nu$. Because, in the wings, $H(a,x) > e^{-x^2}/\sqrt{\pi}$, one finds that the red side of the line profile is slightly enhanced, and the overall profile appears systematically *redshifted* from line-center. This effect, however, is negligibly small for realistic values of a, and the redshift of line-center is given very approximately by

$$\Delta\lambda_0 \;\approx\; 0.035 a^{0.8}\ \text{Å} \quad . \tag{56}$$

APPENDICES

A. Geometrical Coordinate Systems

Define the north pole of the sun along the z axis of a Cartesian coordinate system, position the center of the sun at the origin, and position an observer along the x axis at an infinite distance from the origin. An *observing ray* is defined as a line of constant y and z, parallel to the x axis. The y and z coordinates of the ray are commonly specified by a sun-centered impact parameter b (also denoted as ρ) and a position angle ψ measured counterclockwise from the north pole, and

$$\begin{aligned} y &= -b \sin\psi \\ z &= b \cos\psi \quad . \end{aligned} \tag{A1}$$

The solution to the equation of radiative transfer, eq. (9), is integrated along an observing ray, and various angular vectors are defined at arbitrary points (x, y, z) along this ray:

- The wind velocity $\mathbf{u}$, which is known from empirical models as a vector function of the spherical coordinate position (r, θ, ϕ) of the point in question.
- The incident radiation unit vector $\hat{\mathbf{n}}'$, which points from the solar surface to the point in question.
- The emergent radiation unit vector $\hat{\mathbf{n}}$, which points from the point in question to the observer along the positive x axis. Thus, $\hat{\mathbf{n}} = \hat{\mathbf{e}}_x$.

As derived above in §3, the three geometrical quantities required are the dot products $(\hat{\mathbf{n}} \cdot \hat{\mathbf{n}}')$, $(\mathbf{u} \cdot \hat{\mathbf{n}})$, and $(\mathbf{u} \cdot \hat{\mathbf{n}}')$. Let us define a rotated ("primed") coordinate system which facilitates the calculation of these scalar products. Rotate the coordinate axes so that the new z' axis points outward radially from the wind-point at (x, y, z), or at (r, θ, ϕ), but is still centered on the same origin:

$$\begin{pmatrix} x' \\ y' \\ z' \end{pmatrix} = \begin{pmatrix} \cos\theta\,\cos\phi & \cos\theta\,\sin\phi & -\sin\theta \\ -\sin\phi & \cos\phi & 0 \\ \sin\theta\,\cos\phi & \sin\theta\,\sin\phi & \cos\theta \end{pmatrix} \begin{pmatrix} x \\ y \\ z \end{pmatrix} \quad . \tag{A2}$$

Then, an incident radiation vector $\hat{\mathbf{n}}'$ can be specified by *local* spherical coordinate angles θ' and ϕ' and a unit length of $r' = 1$, and expressed in primed Cartesian coordinates as

$$\hat{\mathbf{n}}' = (\sin\theta' \cos\phi')\hat{\mathbf{e}}_{x'} + (\sin\theta' \sin\phi')\hat{\mathbf{e}}_{y'} + (\cos\theta')\hat{\mathbf{e}}_{z'} \quad . \tag{A3}$$

The coordinate unit vectors $\hat{\mathbf{e}}_{i'}$, where $i = x, y, z$, can then be rotated into the unprimed coordinate system (see, e.g., Arfken & Weber 1995), and

$$\begin{aligned} \hat{\mathbf{n}}' = {} & \hat{\mathbf{e}}_x\,(\cos\theta\,\cos\phi\,\sin\theta'\,\cos\phi' - \sin\phi\,\sin\theta'\,\sin\phi' + \sin\theta\,\cos\phi\,\cos\theta') + \\ & \hat{\mathbf{e}}_y\,(\cos\theta\,\sin\phi\,\sin\theta'\,\cos\phi' + \cos\phi\,\sin\theta'\,\sin\phi' + \sin\theta\,\sin\phi\,\cos\theta') + \\ & \hat{\mathbf{e}}_z\,(-\sin\theta\,\sin\theta'\,\cos\phi' + \cos\theta\,\cos\theta') \quad . \end{aligned} \tag{A4}$$

The dot product $(\hat{\mathbf{n}} \cdot \hat{\mathbf{n}}')$ is then given merely by $\hat{n}'_x$, the unprimed x component of $\hat{\mathbf{n}}'$. In the large-distance limit of a *point source* of radiation (i.e., for $\hat{\mathbf{n}}' = \hat{\mathbf{e}}_r$), we find that $\theta' = 0$, and

$$\hat{\mathbf{n}} \cdot \hat{\mathbf{n}}' = \sin\theta\,\cos\phi = \frac{x}{r} \quad . \tag{A5}$$

For a point at a *finite* distance from the sun, the primed polar angle θ' ranges between 0 and a maximum "limb" value,

$$\theta'_* \;=\; \sin^{-1}\left(\frac{R_\odot}{r}\right) \;\;, \tag{A6}$$

and the primed azimuthal angle ϕ' ranges between 0 and 2π. For a spherically symmetric solar wind model, the integration over $d\Omega' = \sin\theta'\, d\theta'\, d\phi'$ simplifies to $d\Omega' = -2\pi\, d\mu'$, where $\mu' = \cos\theta'$.

The solar wind velocity field is expressed in terms of the above Cartesian unit vectors as

$$\begin{aligned} \mathbf{u} \;\;=\;\; & \hat{\mathbf{e}}_x\,(u_r\,\sin\theta\,\cos\phi + u_\theta\,\cos\theta\,\cos\phi - u_\phi\,\sin\phi) + \\ & \hat{\mathbf{e}}_y\,(u_r\,\sin\theta\,\sin\phi + u_\theta\,\cos\theta\,\sin\phi + u_\phi\,\cos\phi) + \\ & \hat{\mathbf{e}}_z\,(u_r\,\cos\theta - u_\theta\,\sin\theta) \;\;. \end{aligned} \tag{A7}$$

The dot product $(\mathbf{u}\cdot\hat{\mathbf{n}})$ is given by the x component of the above, and does not depend on the primed angles θ' and ϕ'. The dot product $(\mathbf{u}\cdot\hat{\mathbf{n}}')$ can be constructed easily by summing the products of like components of eqs. (A4) and (A7). For the limit of a point source and a radially symmetric wind (i.e., with $\mathbf{u} = u_r\hat{\mathbf{e}}_r$ and $r \gg R_\odot$),

$$\mathbf{u}\cdot\hat{\mathbf{n}}' \;=\; u_r \;\;, \qquad \mathbf{u}\cdot\hat{\mathbf{n}} \;=\; u_r\,\sin\theta\,\cos\phi \;=\; u_r(\hat{\mathbf{n}}\cdot\hat{\mathbf{n}}') \;\;. \tag{A8}$$

B. Atomic Data of Interest to UVCS

A spectral line transition between lower level i and upper level j can occur either radiatively or via collisions with other particles. The rates of spontaneous emission, stimulated emission, and direct absorption of *photons* are denoted A_{ji}, B_{ji}, and B_{ij}, and are coupled by the Einstein relations

$$A_{ji} \;=\; \frac{2h\nu_0^3}{c^2}\,B_{ji} \;\;, \qquad g_i B_{ij} \;=\; g_j B_{ji} \;\;, \tag{B1}$$

where $\nu_0 = c/\lambda_0$ is the frequency of the transition, and g_i and g_j are the statistical weights assigned to levels i and j to account for degenerate sublevels ($g = 2J + 1$). The total opacity in the line, corrected for the effects of stimulated emission, is given by Mihalas (1978) as

$$\begin{aligned} \chi_L^{\rm rad} \;\;&=\;\; \frac{h\nu_0}{4\pi}\,(n_i B_{ij} - n_j B_{ji}) \\ &=\;\; \frac{h\nu_0}{4\pi}\,g_i B_{ij}\,(n_i/g_i - n_j/g_j) \\ &\approx\;\; \frac{h\nu_0}{4\pi}\,n_i B_{ij}\,[1 - (b_j/b_i)\exp(-h\nu_0/kT)] \;\;, \end{aligned} \tag{B2}$$

where n_i and n_j are the number densities (in cm^{-3}) of ions in levels i and j, and the last equality above applies for the general non-LTE case. However, in the solar corona, atomic ground states are highly overpopulated relative to the neighboring excited states, and we can safely assume that the ratio of departure coefficients from LTE (b_j/b_i) approaches zero. Also, the absorption rate B_{ij} can be expressed as a quantum mechanical *oscillator strength* f_{ij}

$$\frac{h\nu_0}{4\pi}B_{ij} \;=\; \frac{\pi e^2}{m_e c}\,f_{ij} \;\;, \tag{B3}$$

and the above quantities are effective cross sections per unit time (in cm^2 s^{-1}) for scattering of photons from the atom or ion. In Table 1, below, we list various intrinsic quantities, including the transition rates A_{ji}, for a subset of line transitions of interest to UVCS observations. The energy levels and transition rates come from the revised Opacity Project data of Verner et al. (1996). For the Hydrogen Lyman series lines we list

averaged quantities for the closely-spaced hyperfine doublet, but for other lines we list each component of doublets separately.

Many lines are affected by collisions with atoms, ions, and electrons. However, only the *electrons* usually need to be considered, because in thermal equilibrium their flux (proportional to velocity) is larger than that of atoms and ions by at least an order of magnitude. The rates of collisional excitation and de-excitation are given by C_{ij} and C_{ji}, and the latter is analogous to the radiative rate A_{ji}. Collisions affect the *thermalization* of a given line via the parameter

$$\varepsilon \;=\; \frac{C_{ji}(1-\exp[-h\nu_0/kT])}{A_{ji}+C_{ji}(1-\exp[-h\nu_0/kT])} \;\;, \tag{B4}$$

which is much less than unity for most lines of interest. However, in the source function (eq. [4]), the thermalized fraction of a line's opacity is multiplied by the Planck function, which can be many orders of magnitude larger than the *incident* radiation that multiplies the scattered (non-thermalized) fraction of the opacity.

If we assume that, when averaged over a large enough ensemble, every collision occurs along with its opposite (i.e., "detailed balance"), then

$$n_i C_{ij} \;=\; n_j C_{ji} \;\;, \tag{B5}$$

or, for a thermal equilibrium distribution of electrons (equivalent to LTE for photons),

$$\frac{C_{ij}}{C_{ji}} \;=\; \frac{g_j}{g_i}\,\exp[-h\nu_0/kT] \;\;. \tag{B6}$$

Also, because the collision rate is dependent on the density and energy (or temperature) of the electrons, we can write

$$C_{ij} \;=\; n_e\, q_{ij}(T_e) \;\;. \tag{B7}$$

The collision rate per electron q_{ij} (which represents an average or moment over the electron velocity distribution, assumed Maxwellian) can be computed to various degrees of accuracy. Current work with UVCS data utilzes updated rates compiled by Raymond et al. (1997), but let us present here a simpler closed-form expression that agrees to within $\sim$ 20–30% with the best modern values. Mihalas (1978) gives a slightly modified form of Van Regenmorter's (1962) fit for electron impact excitation rates in radiatively permitted transitions, and

$$q_{ij} \;\approx\; 14.5\,\pi a_0^2 \sqrt{\frac{8kT_e}{m_e\pi}}\, f_{ij} \left(\frac{I_H}{h\nu_0}\right)^2 u_0\, e^{-u_0}\; \max[\bar{g}, 0.276 e^{u_0} E_1(u_0)] \;\;, \tag{B8}$$

where a_0 is the Bohr radius, I_H is the ionization energy of Hydrogen, $u_0 \equiv h\nu_0/kT_e$, and $\bar{g}$ is an effective Gaunt factor which is $\sim$0.7 for transitions of the form $n\ell \rightarrow n\ell'$, and $\sim$0.2 for transitions of the form $n\ell \rightarrow n'\ell'$.

Table 2 contains representative values of the thermalization parameter ε, computed from the above q_{ij} approximation, and for fiducial solar corona parameters: $n_e = 10^7\,\mathrm{cm}^{-3}$ and $T_e = 1.5 \times 10^6\,\mathrm{K}$. Also, in Table 2 are listed representative quiet-sun values for the incident (chromospheric) line intensities, taken from various sources and subject to change for any individual set of observations. We temporarily neglect the limb darkening or brightening of coronal line strengths. The six listed parameters represent fitting parameters in the following general (two Gaussians + one quasi-Lorentzian) function:

$$I_\nu(\mathrm{chromosphere}) \;=\; I_a \exp[-(\Delta\lambda/w_a)^2] \;+\; I_b \exp[-(\Delta\lambda/w_b)^2] \;+\; \frac{I_c}{1+|\Delta\lambda/w_c|^{2.5}} \tag{B9}$$

where $\Delta\lambda = \lambda - \lambda_0$, the line-center intensities I_a, I_b, and I_c are listed in units of 10^{-10} erg s^{-1} cm^{-2} sr^{-1} Hz^{-1}, and w_a, w_b, and w_c are in Ångstroms. Finally, the total line-center incident intensity ($I_a + I_b + I_c$) is

used to compute a "realistic" estimate of how collisionally dominated each line will be for the above fiducial density and temperature:

$$\Psi \equiv \frac{\varepsilon B_{\nu_0}(T_e)}{(1-\varepsilon)(I_a + I_b + I_c)} \ . \tag{B10}$$

Note the hidden *electron density* sensitivity in this ratio, since one can show that

$$\varepsilon B_\nu \ = \ (C_{ij}/B_{ij}) \ = \ (n_e q_{ij}/B_{ij}) \ . \tag{B11}$$

Thus, lines formed in, e.g., denser coronal streamers or active regions, compared to less-dense coronal holes, will have a larger fraction of their emission caused by collisions.

REFERENCES

Arfken, G. B., & Weber, H. J. 1995, Mathematical Methods for Physicists, 4th ed. (San Diego: Academic Press)

Beckers, J. M., & Chipman, E. 1974, Sol. Phys., 34, 151

Chandrasekhar, S. 1960, Radiative Transfer (New York: Dover)

Collins, II, G. W. 1989, The Fundamentals of Stellar Astrophysics (New York: Freeman)

Cram, L. E., & Vardavas, I. M. 1978, Sol. Phys., 57, 27

Cranmer, S. R. 1997, ApJ, in preparation

Dirac, P. A. M. 1925, MNRAS, 86, 825

Dreicer, H. 1959, Phys. Rev., 115, 238

House, L. L. 1970, J. Quant. Spectrosc. Radiat. Transfer, 10, 909

Hummer, D. 1962, MNRAS, 125, 21

Hundhausen, A. J. 1972, Coronal Expansion and Solar Wind (Berlin: Springer-Verlag)

Hyder, C. L., & Lites, B. W. 1970, Sol. Phys., 14, 147

Kohl, J. L., Esser, R., Gardner, L. D., Habbal, S., Daigneau, P. S., Dennis, E. F., Nystrom, G. U., Panasyuk, A., Raymond, J. C., Smith, P. L., Strachan, L., van Ballegooijen, A. A., Noci, G., Fineschi, S., Romoli, M., Ciaravella, A., Modigliani, A., Huber, M. C. E., Antonucci, E., Benna, C., Giordano, S., Tondello, G., Nicolosi, P., Naletto, G., Pernechele, C., Spadaro, D., Poletto, G., Livi, S., von der Lühe, O., Geiss, J., Timothy, J. G., Gloeckler, G., Allegra, A., Basile, G., Brusa, R., Wood, B., Siegmund, O. H. W., Fowler, W., Fisher, R., & Jhabvala, M. 1995, Sol. Phys., 162, 313

Kohl, J. L., Strachan, L., & Gardner, L. D. 1996, ApJ, 465, L141

Kohl, J. L., & Withbroe, G. L. 1982, ApJ, 256, 263

Kopp, R. A., & Holzer, T. E. 1976, Sol. Phys., 49, 43

Leer, E., Holzer, T. E., & Flå, T. 1982, Space Sci. Rev., 33, 161

McKenna, S. 1984, Ap&SS, 107, 71

Mihalas, D. 1978, Stellar Atmospheres, 2nd ed. (San Francisco: W. H. Freeman)

Mihalas, D., & Mihalas, B. W. 1984, Foundations of Radiation Hydrodynamics (Oxford: Oxford U. Press)

Noci, G., Kohl, J. L., & Withbroe, G. L. 1987, ApJ, 315, 706

Olsen, E. L., Leer, E., & Holzer, T. E. 1994, ApJ, 420, 913

Parker, E. N. 1958, ApJ, 128, 664

Table 1: Basic Atomic Data

Ion	Transition	λ_0 (Å)	g_i	g_j	A_{ji} (s^{-1})	$(h\nu_0/4\pi)B_{ij}$ ($cm^2\ s^{-1}$)
H I (Lα)	1s – 2p	1215.6700	2	6	6.26×10^8	1.104×10^{-2}
H I (Lβ)	1s – 3p	1025.7222	2	6	1.67×10^8	2.097×10^{-3}
H I (Lγ)	1s – 4p	972.5367	2	6	6.82×10^7	7.700×10^{-4}
C II	$2s^2\ 2p$ – $2s\ 2p^2$	1037.0182	4	2	1.53×10^9	3.273×10^{-3}
O VI	$1s^2\ 2s$ – $1s^2\ 2p$	1037.6167	2	2	4.09×10^8	1.752×10^{-3}
O VI	$1s^2\ 2s$ – $1s^2\ 2p$	1031.9261	2	4	4.17×10^8	3.534×10^{-3}
Mg X	$1s^2\ 2s$ – $1s^2\ 2p$	624.9410	2	2	7.00×10^8	1.088×10^{-3}
Mg X	$1s^2\ 2s$ – $1s^2\ 2p$	609.7930	2	4	7.55×10^8	2.234×10^{-3}
Si XII	$1s^2\ 2s$ – $1s^2\ 2p$	520.6650	2	2	8.49×10^8	9.158×10^{-4}
Si XII	$1s^2\ 2s$ – $1s^2\ 2p$	499.4060	2	4	9.61×10^8	1.907×10^{-3}

Table 2: Collisional and Incident Intensity Data

Ion	ε	I_a	w_a	I_b	w_b	I_c	w_c	Ψ
H I λ1215	1.393×10^{-11}	800	0.210	-600	0.072	80	0.7	0.00134
H I λ1025	9.227×10^{-12}	11.5	0.260	-8.0	0.12	0.50	0.7	0.0866
H I λ972	8.098×10^{-12}	1.05	0.290	0	0	0	0	0.321
C II λ1037	1.158×10^{-9}	1.27	0.072	0	0	0	0	0.335
O VI λ1037	1.159×10^{-11}	3.31	0.101	0	0	0	0	0.129
O VI λ1032	1.146×10^{-11}	6.55	0.101	0	0	0	0	0.0649
Mg X λ625	4.079×10^{-12}	0.871	0.038	0	0	0	0	0.460
Mg X λ610	3.875×10^{-12}	3.21	0.038	0	0	0	0	0.124
Si XII λ521	2.788×10^{-12}	0.476	0.029	0	0	0	0	0.815
Si XII λ499	2.555×10^{-12}	0.776	0.029	0	0	0	0	0.496

Parker, E. N. 1963, Interplanetary Dynamical Processes (New York: Interscience Publishers)

Parker, E. N. 1966, ApJ, 143, 32

Pneuman, G. W., & Kopp, R. A. 1971, Sol. Phys., 18, 258

Press, W. H., Flannery, B. P., Teukolsky, S. A., & Vetterling, W. T. 1989, Numerical Recipes: The Art of Scientific Computing (Cambridge: Cambridge U. Press)

Raymond, J. C., Kohl, J. L., Noci, G., Antonucci, E., Tondello, G., Huber, M. C. E., Gardner, L. D., Nicolosi, P., Fineschi, S., Romoli, M., Spadaro, D., Siegmund, O. H. W., Benna, C., Ciaravella, A., Cranmer, S., Giordano, S., Karovska, M., Martin, R., Michels, J., Modigliani, A., Naletto, G., Panasyuk, A., Pernechele, C., Poletto, G., Smith, P. L., Suleiman, R. M., Strachan, L., and van Ballegooijen, A. A. 1997, Sol. Phys., submitted

Scudder, J. D. 1992a, ApJ, 398, 299

Scudder, J. D. 1992b, ApJ, 398, 319

Strachan, L., Kohl, J. L., Weiser, H., Withbroe, G. L., & Munro, R. H. 1993, ApJ, 412, 410

Van Regenmorter, H. 1962, ApJ, 136, 906

Verner, D. A., Verner, E. M., & Ferland, G. J. 1996, Atomic Data Nucl. Data Tables, 64, 1

Withbroe, G. L. 1970, Sol. Phys., 11, 42

Withbroe, G. L., Kohl, J. L., Weiser, H., & Munro, R. H. 1982, Space Sci. Rev., 33, 17

Zanstra, H. 1946, MNRAS, 106, 225